Volume 18, Number 2, 2025. pp. 113-122

Jordan Journal of Physics

ARTICLE

Electronic and Optical Properties of Zr-, Zr-N-doped 2D MoS_2 Using First-Principle Study

A. Ouahdani, R. Takassa, A. E. Mouncharih, F. Elfatouaki, O. Farkad, S. Hassine, O. Choukri, E.A. Ibnouelghazi and **D. Abouelaoualim**

LaMEE, Department of Physics, Faculty of Sciences Semlalia, Cadi Ayyad University, P.O. Box 2390, 40000 Marrakech, Morocco.

Doi: **https://doi.org/10.47011/18.2.1**

Received on: 09/07/2023; *Accepted on: 18/02/2024*

Abstract: A MoS_2 monolayer is an emerging two-dimensional (2D) semiconductor for next-generation flexible and miniaturized electronics. Its doping is of great importance in order not only to adapt its properties, but also to facilitate many potential large-scale applications. In this work, density functional theory (DFT) calculations, including spin-orbit coupling (SOC), were performed to investigate the effects of p-type transition metal Zr doping and Zr–N co-doping on the structural and optoelectronic properties of pristine MoS_2. Results obtained using both the PBE and TB-mBJ approximations show that while pristine and Zr-doped MoS_2 monolayers exhibit semiconductor behavior with direct and indirect band gaps, respectively, Zr-N co-doping leads to a transition to metallic behavior. The Zr and N atoms significantly affect the partial and total density of state profiles, with a main contribution of Zr − d, N − p, and S − p orbitals. The dielectric function and optical refractive index are also determined. The findings show anisotropy in optical characteristics, which is promising for optical applications. The Zr-doping and Zr-N co-doping employed in this study provide an effective tool for changing the electrical and optical properties of MoS_2 monolayers to fulfill the needs of a variety of technological applications while producing an optoelectronic device based on a MoS_2 monolayer.

Keywords: MoS_2 monolayer, Zr doped, Zr-N co-doped, DFT study, Electronic properties, Dielectric function.

1. Introduction

The most significant molybdenum mineral is molybdenum disulfide (MoS_2) [1], which occurs naturally as molybdenite. MoS_2 belongs to the VIB group of the transition metal dichalcogenide (TMDC) monolayers and is one of the most highly debated 2D materials in recent times, second only to graphene [2, 3], due to its easy synthesis, low cost, nontoxicity, and natural abundance [4]. These layered materials have attracted attention due to their weak van der Waals interactions that allow to fabricate them easily using mechanical exfoliation [5, 6]. Researchers reexamined this type of material and succeeded in obtaining atomic-level two-dimensional layered MoS_2 [7-12]. As a typical graphene-like single-layer transition metal compound, single-layer molybdenum disulfide exhibits a substantial band gap ranging from 1.3 to 1.8 eV [13], making it suitable for applications such as transistors [14,15], solar energy harvesting [16], flexible optoelectronic devices [17], and sensors [18]. Lahourpour *et al.* [12] used full potential linear augmented plane waves plus local orbital (FP-LAPW + lo) method based on the DFT technique to study MoS_2 nanolayers. Their findings reveal that the estimated lattice parameters overshoot the actual values, which is a characteristic of the typically

Corresponding Author: D. Abouelaoualim **Email**: dr.abouelaoualim@uca.ac.ma

generalized gradient approximation GGA-PBE functional. Furthermore, they demonstrated that MoS_2 exhibits semiconductor behavior, revealing a direct band gap of 1.72 eV at the K point of the Brillouin zone, consistent with both experimental observations [19] and theoretical predictions [20, 21]. In recent years, numerous studies have been conducted on the structural, electronic, and optical properties of doped MoS_2. The effect of doping with nonmetallic atoms (X = O, C, N, B, Br, Cl, I, and F) using DFT calculations on the structural, electrical, and magnetic properties of single-layered MoS_2 has been investigated. The outcomes indicated that the systems doped with B, C, and N exhibit p-type doping, while the halogen-doped systems demonstrate n-type doping. [21]. The interactions with water molecules (H_2O), carbon dioxide (CO_2), and sulfur dioxide (SO_2) with MoS_2 monolayers doped with Ru and Rh have also been investigated using DFT calculations. The investigation revealed the preferred configuration for the adsorption geometry of SO_2 on the monolayer Ru-MoS_2 [11]. In contrast, Qian *et al.* [16] employed Au as a dopant to modify both the structural and electronic characteristics of MoS_2 fiber materials. Their study utilized DFT theory to investigate the adsorption effectiveness of Au-doped MoS_2 towards gases such as C_2H_6 and C_2H_4. The results indicated that the presence of Au dopant particles enhances the adsorption capability of the MoS2 monolayer by influencing its electronic structure. Furthermore, Xu *et al*. [22] conducted DFT computations to investigate the electronic and optical properties of co-doped monolayers of MoS_2 with C, N, B, and Mn. The co-doped systems containing Mn-N and Mn-B atoms exhibited semiconducting behavior, with energy band gaps of 0.81 and 1.03 eV, respectively. Recently, Raza *et al.* [23] studied the electronic properties of doped monolayers of MoS_2 with transition metals (Ag, Co, Bi, and Zr) using a local combination of atomic orbitals (LCAO) approach within the framework of DFT calculations. They confirmed that doping with transition metals led to a reduction in the band gap to a certain extent.

In the present study, we extend the exploration of electronic and optical properties of MoS_2 monolayers through DFT calculations utilizing the full-potential linearized augmented plane wave (FP-LAPW) method. We introduce p-type transition metal Zr atoms and explore both Zr doping and Zr–N co-doping as strategies to modulate the electronic and optical behavior of MoS_2. This choice is motivated by previous findings showing that such dopants effectively tune the physical properties of other 2D transition metal dichalcogenide (TMD) materials [24–26]. This research introduces a new perspective by examining the effects of Zr doping and Zr-N co-doping on the practical applications of doped MoS_2 monolayers as potential optoelectronic materials.

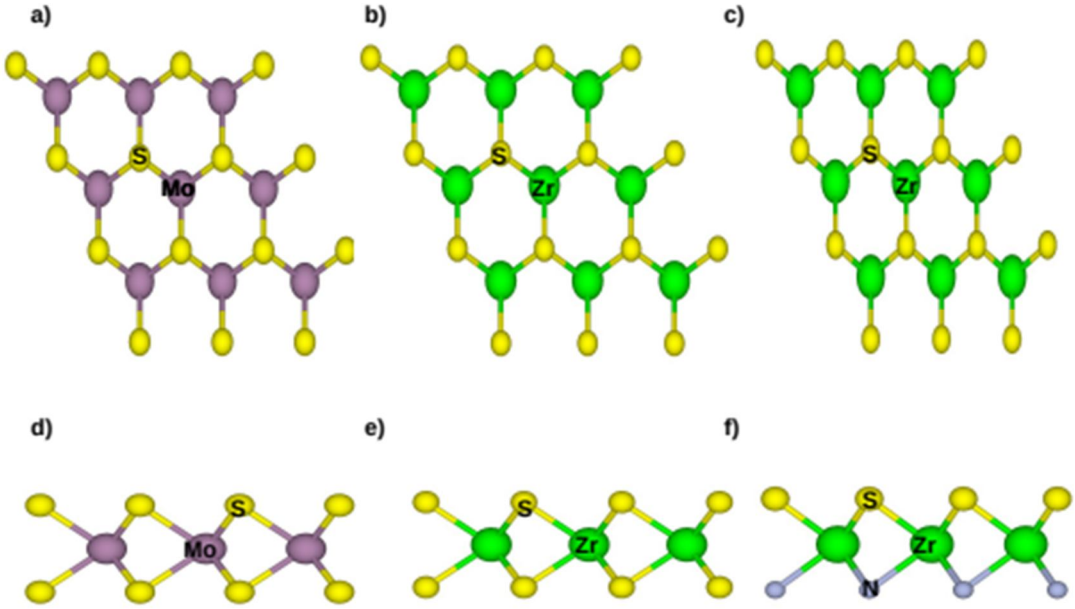

FIG. 1. Optimized geometric structures of the MoS_2 monolayer: (a) top view and (d) side view of the pristine MoS_2 monolayer; (b) top view and (e) side view of the Zr-doped MoS_2 monolayer; (c) top view and (f) side view.

2. Computational Method

This article examines the impact of Zr doping and Zr-N co-doping on the monolayer of MoS_2, as illustrated in Fig.1. To characterize the structural, electronic, and optical properties of both the pristine and doped MoS_2 monolayers, DFT and FP-LAPW method [27-29] are employed using the WIEN2K code [30]. The generalized gradient approximation in the form of the Perdew-Burke-Ernzerhof (GGA-PBE) and Tran-Blaha modified Becke-Johnson (TB-mBJ) [31, 32] is employed to approximate the exchange-correlation (XC) energy functional, accounting for the presence of SOC effects, without including the van der Waals correction due to weak van der Waals interactions [5]. The muffin-tin (MT) radii for Mo, S, Zr, and N are chosen as 2.42, 2.05, 2.40, and 2.00 a.u., respectively. A plane wave cut-off value of $R_{MT} \times K_{max} = 7$ was chosen for the wave function in the interstitial region. Here, R_{MT} represents the smallest radius of the atomic sphere, and K_{max} denotes the largest k-vector in the plane wave expansion. The cut-off energy of -6 Ry was consistently maintained to distinguish the core and valence states. The maximum angular momentum for the atomic orbital basis functions was specified as $l_{max} = 10$. The Fourier expansion's charge density was terminated at $G_{max} = 12$. Throughout the calculations, a 3 × 3 × 1 supercell was employed for both the pristine and doped MoS_2 monolayers in the x-y plane. Periodic boundary conditions were applied, while ensuring a minimum vacuum space of 15 Å along the z-axis to prevent interactions between adjacent layers. The first Brillouin zone (BZ) was sampled using a total of 1000 k-points. The iteration process was concluded when the total energy reached a threshold of 10^{-4} Ry. The random phase approach (RPA) was utilized to compute the optical properties. [33]. The optical spectra's intensity was controlled by dipole selection criteria, which differentiate optically permitted and prohibited transitions [34]. The Kramers-Kronig transformation yielded the real part ε_1 [35] and then the optical refraction index. An additional Drude term was included to account for free-electron intraband input in metallic structures. For accurate evaluation of optical response properties, a denser k-point mesh of 9 × 9 × 58 (equivalent to 5000 k-points in the BZ) was employed [34].

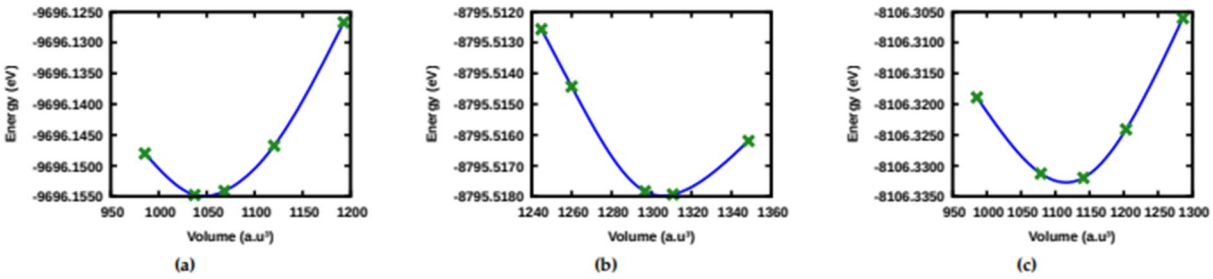

FIG. 2. Optimized energy-volume curves for (a) pristine, (b) Zr-doped, and (c) Zr-N c-doped MoS_2.

3. Numerical Results and Discussion

3.1. Structural Properties and Stability

A 3 × 3 × 1 supercell comprising 27 atoms with hexagonal symmetry was constructed using the supercell approach to model the pristine MoS_2, Zr-doped MoS_2 (ZrS_2), and Zr–N co-doped MoS_2 (ZrSN) structures. The unit cell of a MoS_2 monolayer consists of one Mo atom and two S atoms. In the case of ZrS_2, one Mo atom is substituted with a Zr atom. For the ZrSN structure, one Mo atom is replaced by a Zr atom and one S atom by an N atom, as illustrated in Fig. 1. To determine the stability and ground-state properties of the pristine and doped structures, energy minimization was performed using the generalized gradient approximation (GGA-PBE) in conjunction with the Murnaghan equation of state, expressed as [39]:

$$E(V) = E_0 + \left[\frac{B_0 V}{B_0'}\left(\frac{(V_0/V)^{B_0'}}{B_0'-1}+1\right) - \frac{B_0 V}{B_0'-1}\right]\frac{1}{14703.6} \quad (1)$$

Figure 2 shows the plot of total energy versus volume. Here, E_0, V, V_0, B_0, and B_0' are the minimum energy at T = 0 K, unit cell volume, unit cell volume at P = 0 GPa, bulk modulus, and its pressure derivative, respectively. The crystal structures and the estimated ground-state parameters of all configurations are shown in Table 1. The results show that the pristine MoS_2, Zr-doped, and Zr-N c-doped MoS_2 structures crystallize in hexagonal structures with space

groups P-6m2 (No. 187), P-6m2 (No. 187), and P3m1 (No. 156), respectively. The theoretically optimized lattice parameters for the pristine MoS_2 monolayer unit cell are a = b = 3.19Å, consistent with prior experimental and theoretical values, as shown in Table.1. After Zr doping and Zr-N co-doping, the Zr-S and Zr-N bond lengths become larger than in the case of Mo-S, which can be explained by the difference in the radii of Mo, Zr, S, and N atoms. To validate the thermodynamic stability, the formation energies of all compounds are calculated using the following equation [40], which is deduced experimentally for semiconducting materials in any form:

$$E_f = E_{tot}(X) - E_{tot}(MoS_2) - n_i\mu_i \quad (2)$$

$E_{tot}(X)$ and $E_{tot}(MoS_2)$ serve as representations of the total energy for the doped and pristine MoS_2 monolayers, respectively. The term $n_i > 0$ represents the number of doped atoms, while $n_i < 0$ represents the number of replaced atoms from the MoS_2 monolayer. The chemical potential of a single atom, which is determined as the overall energy per atom of the element's most stable structure, is represented by μ_i. The negative formation energies observed in Table 1 indicate the thermodynamic stability of the doped compounds, suggesting the feasibility of material synthesis. In addition, the Zr-N co-doped MoS_2 structure is more stable than Zr-doped MoS_2 because it presents a smaller formation energy value.

TABLE 1. Space groups, lattice parameters (a, b, c), unit cell volume at P = 0 GPa (V0), bulk modulus (B0), pressure derivative of bulk modulus (B 0 0), formation energy (E_f), and band gap with approximations PBE and TB-mBJ (Eg) for pristine, Zr-doped, and Zr-N co-doped MoS2 monolayers.

	Space group	bond length (Å)	$a = b$ (Å)	c (Å)	V_0 (Å^3)	B_0 (GPa)	B_0'	E_f (eV)	E_g (eV)
MoS_2	P-6m2	$d_{(Mo-S)}$= 2.42	3.19	17.46	1046.001	51.672	4.713	-	1.66_{PBE}
									1.63_{TB-mBJ}
		2.38 [36]	3.16 [36]						1.66 [37]
		2.42 [22]	3.17 [37]						1.80 [38]
									1.79 [36]
Zr / MoS_2	P-6m2	$d_{(Zr-S)}$= 2.59	3.55	17.46	1308.645	46.512	5.000	-1.39	0.99_{PBE}
									1.14_{TB-mBJ}
Zr-N / MoS_2	P3m1	$d_{(Zr-S)}$=2.45	3.36	16.40	1107.009	28.343	0.200	-4,62	0_{PBE}
		$d_{(Zr-N)}$= 2.45							0_{TB-mBJ}

3.2 Electronic Properties

3.2.1 Electronic Band Structure and Band Gap

To fully understand the optoelectronic behavior of semiconductors, it is essential to examine their electronic structure. The electronic band structures were computed using the GGA-PBE approximation while accounting for spin–orbit coupling (SOC) effects. The nature of the band gap, whether direct or indirect, is a critical factor in determining a material's suitability for optoelectronic applications.

The calculated band structures using both PBE and TB-mBJ approximations, along the high-symmetry points in the Brillouin zone (BZ), are presented in Fig. 3. Analysis of the pristine MoS_2 monolayer reveals that both the valence band maximum (VBM) and the conduction band minimum (CBM) occur at the K point, as seen in Figs. 3(a) and 3(d), indicating a direct band gap under both approximations. This confirms that the undoped MoS_2 monolayer is a promising candidate for optoelectronic applications. The estimated band gaps are 1.66 eV (PBE) and 1.63 eV (TB-mBJ), which are in good agreement with experimental values [19].

However, upon Zr doping, a transition from a direct to an indirect band gap is observed, accompanied by a reduction in band gap energy to 0.99 eV (PBE) and 1.14 eV (TB-mBJ), as shown in Figs. 3(b) and 3(e). This suggests that Zr-doped MoS_2 may be less suitable for optoelectronic devices.

In contrast, co-doping with Zr and N atoms eliminates the band gap entirely, reducing it to 0 eV under both approximations. This transition indicates a metallic behavior for the Zr–N co-doped MoS_2, as presented in Figs. 3(c) and 3(f).

3.2.2 TDS and PDOS

Partial (PDOS) and total density of states (TDOS) calculations were carried out to comprehend the role that Zr and N atoms played in the formation of the valence band VB and conduction band (CB) energies for the compound MoS_2, as well as any potential hybridization and interactions between these atoms. Fig. 4 presents the computed TDOS and PDOS of pristine, Zr-doped, and Zr–N co-doped MoS_2 monolayers over the energy range from -5 to 5 eV, using the PBE exchange–correlation (XC) approximation. The VB and CB are divided by the Fermi level, which has a value of 0.0 eV. The results show that the choice of the doping manner and the two Zr and N atoms significantly affect the DOS and PDOS profiles. Indeed, significant effects are observed in the TDOS profile in the energy range of -5 eV to 0 eV. By doping with the Zr atom, the gap value width decreased, as shown in Figs. 4(a) and 4(b), which is due to the d orbital of Zr dominating the conduction band and which was dominated by Mo − d and S − p orbitals [Figs. 4(d) and 4(e)], with a clear annulment of the states in the interval from 2.5 to 3.4 eV, which plays a crucial role in defining the material's electronic behavior. While the valence band is strongly dominated by p-orbitals in both structures, with an annuity of states in -5 to 5 eV in the doped structure. For the third compound, substitution of Mo by Zr and S by N gives a different curve shape. The conduction band retains its structure with a slight diminution in the number of states/eV, and the gap width decreased by 0.25 eV from that of the Zr-doped structure, as presented in Fig. 4(c).

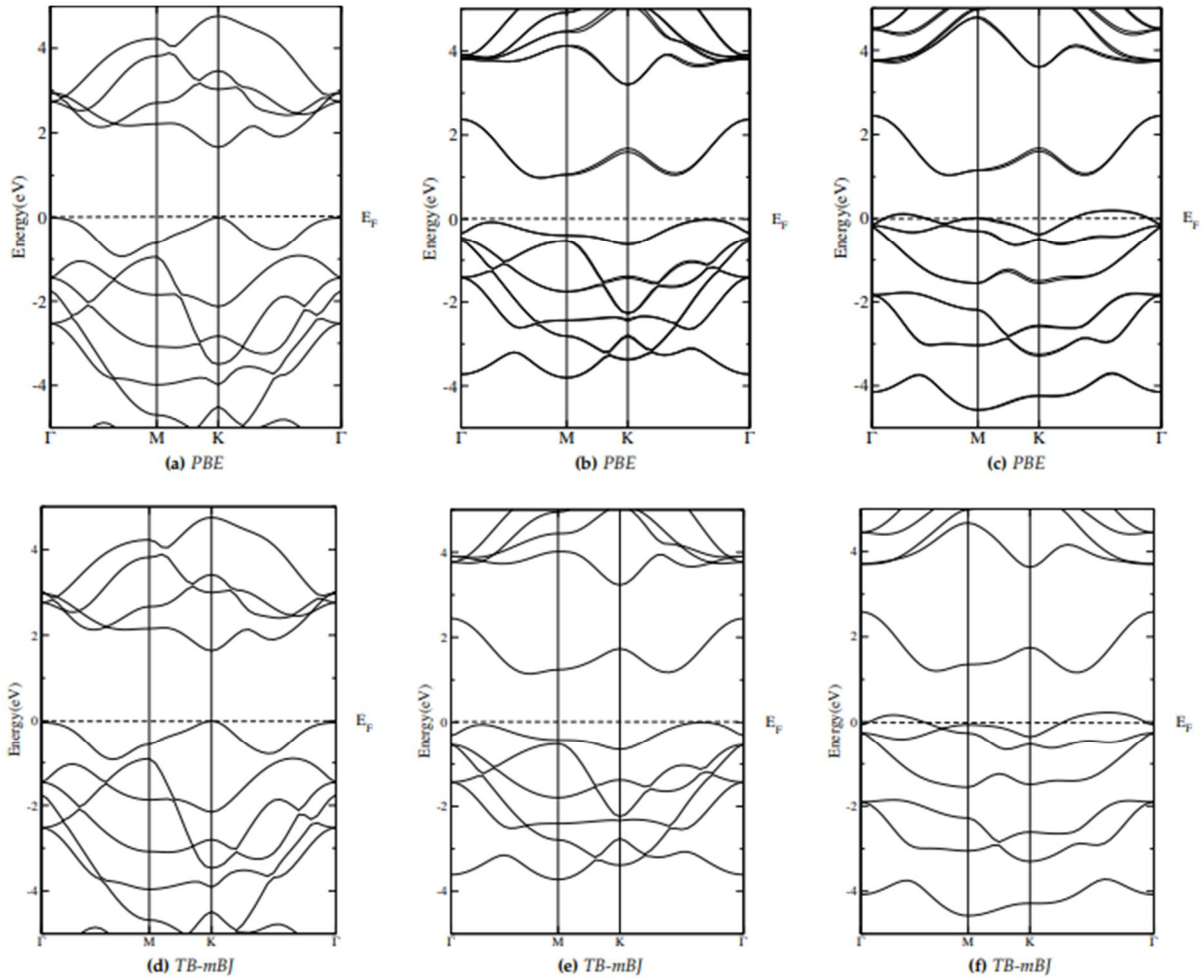

FIG. 3. Calculated band structures using PBE and TB-mBJ approximations for (a), (d) pristine, (b), (e) Zr-doped, and (c), (f) Zr-N co-doped MoS_2.

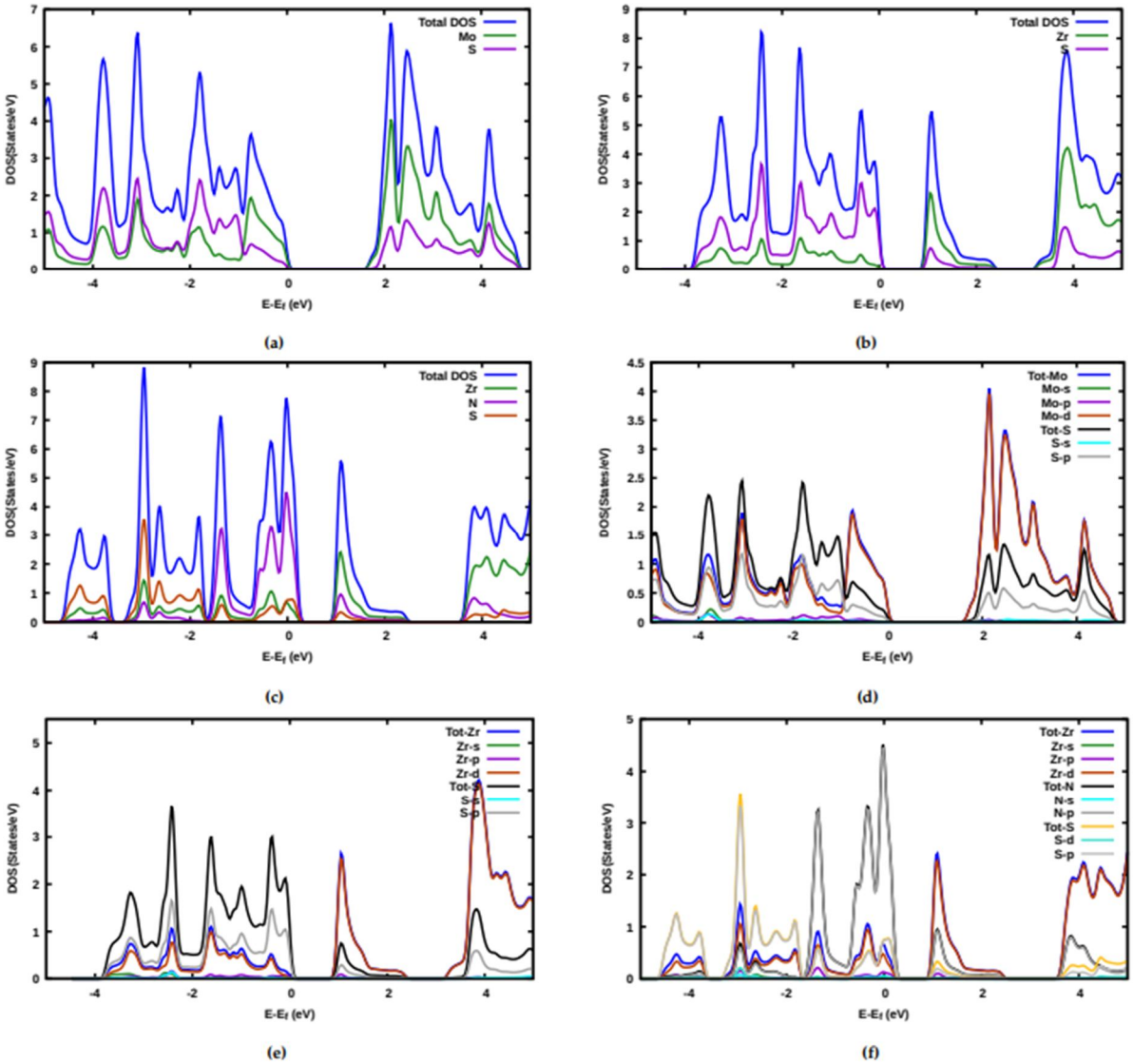

FIG. 4. Calculated total and partial DOS of (a), (d) pristine, (b), (e) Zr-doped, and (c), (f) Zr-N co-doped MoS_2.

This band gap is primarily formed from the d-states of Zr, p-states of N, and p-states of S. Yet, the valence band has undergone a clear change: it has displaced the Fermi level from -2 to 0.25 eV. The N − p orbital is the major contributor, as evidenced by the increased intensity of the observed peaks. In the energy range from -4 to 2 eV, S − p is the dominant orbital, as shown in Fig. 4(f). The contribution from the Zr − d orbitals is smaller, indicating that the hybridization of these atoms occurs mainly between the N − p and S − p orbitals, introducing a strong interaction between them, and they are responsible for the observed TDOS profile. In contrast, the s orbitals of each atom show a weak contribution.

3.3 Optical Properties

3.3.1 Dielectric Function

Investigating the optical properties provides valuable insight into the interaction of materials with electromagnetic radiation [41]. These properties are essential for the design and optimization of photoelectronic devices and semiconductor-based technologies. In this work, the optical characteristics were calculated using the random phase approximation (RPA) within the framework of DFT [42]. This approximation considers only the interband transitions between the valence and conduction bands, neglecting the local field effects [42–44]. The substitutional doping with Zr and co-doping with Zr–N alters the structural parameters and modifies the band structures of MoS_2 (see Fig. 3), which consequently affects the optical transitions. These transitions are captured through the

complex dielectric function ε(ω), which characterizes the linear optical response of the system. The dielectric function consists of a real part, $\varepsilon_1(\omega)$ and an imaginary part, $\varepsilon_2(\omega)$, as shown in the following equation:

$$\varepsilon(\omega) = \varepsilon_1(\omega) + i\varepsilon_2(\omega) \quad (3)$$

Once the ε(ω) is obtained, many other interesting optical properties can be deduced. The $\varepsilon_1(\omega)$ and $\varepsilon_1(\omega)$ for various materials of the pristine, Zr-doped, and Zr-N co-doped MoS_2 monolayers were estimated using the RPA method as implemented in the Wien2k package. Calculations were performed for two polarization directions: parallel (xx) and perpendicular (zz), denoted as $\varepsilon^{\parallel}(\omega)$ and $\varepsilon^{\perp}(\omega)$, respectively. Figs. 5 and 6 demonstrate that ε(ω) exhibits anisotropic behavior for two distinct polarizations of the light. The curves of $\varepsilon_2(\omega)$, shown in Fig. 5, indicate that the threshold energy (optical gap) occurs at 1.8, 0.8 eV, and 2.5, 0.5 eV for pure and Zr-doped MoS_2 monolayer for both polarization xx and zz directions, respectively, while the Zr-N co-doped MoS_2 monolayer exhibits no optical gap. It can be seen that the doped and co-doped MoS_2 monolayer process decreases the optical gap by generating permissible states in the MoS_2 monolayer band gap. As a result, the MoS_2 monolayer exhibits an adjustable band gap. The absorption transitions from the valence bands to the conduction bands are represented by the peaks observed in the $\varepsilon_2(\omega)$. Additionally, the MoS_2 monolayer $\varepsilon_2(\omega)$ shows one main peak at 2.86 eV (visible region) and 5.36 eV (UV region), for the xx and zz polarization directions, respectively. At the same time, the $\varepsilon_2^{\parallel}$ exhibits four prominent peaks at 1.74, 3.65, 3.91, and 4.78 eV and 0.35, 1.22, 4.00, and 6.26 eV, for the Zr-doped and Zr-N co-doped MoS_2 monolayers, respectively. On the other hand, the $\varepsilon_2^{\perp}$shows four main peaks at 1.40, 5.65, 6.26, and 7.30 eV and 2.96, 4.00, 5.65, and 5.91 eV, for the Zr-doped and Zr-N co-doped MoS2 monolayers, respectively. All peaks are formed by π to π ∗, σ to σ ∗, and σ to π ∗ transitions. Fig. 6 presents $\varepsilon_1(\omega)$, showing several peaks across the IR, VL, and UV regions. The $\varepsilon_1(\omega)$ response also varies with doping and co-doping and exhibits noticeable anisotropy in both polarization directions for all investigated models.

3.3.2 Refraction Index

The complex refractive index, denoted as N(ω), characterizes how electromagnetic waves propagate through a material relative to a vacuum. It is calculable using the following relationship [45]:

$$N(\omega) = n(\omega) + ik(\omega) \quad (4)$$

For optical devices, the extinction coefficient is k(ω) while the value of the refractive index is represented by n(ω). Fig. 7 displays the spectra of n(ω) and k(ω), both calculated using the GGA-PBE approximation for MoS_2, Zr-doped MoS_2, and Zr-N co-doped MoS_2. The n(ω) plot indicates the anisotropic behavior, as seen in Fig. 7. The static refractive index, n(0), is one of several key elements in $\varepsilon_1(\omega)$, and it is given by [46]:

$$n(0) = \sqrt{\varepsilon_1(0)} \quad (5)$$

The computed values of n(0) in both parallel and perpendicular orientations are shown in the Table. 2. In the case of the parallel mode, the findings reveal that MoS_2, Zr-doped MoS_2, and Zr-N co-doped MoS_2 exhibit semiconducting and insulating behaviors. In contrast, in the perpendicular direction, all studied structures exhibit typical semiconducting behavior.

Additionally, the results show that after Zr doping and Zr–N co-doping, n(0) increases in the parallel direction but decreases in the perpendicular direction. This is because the refractive index is inversely related to the band gap of the compound.

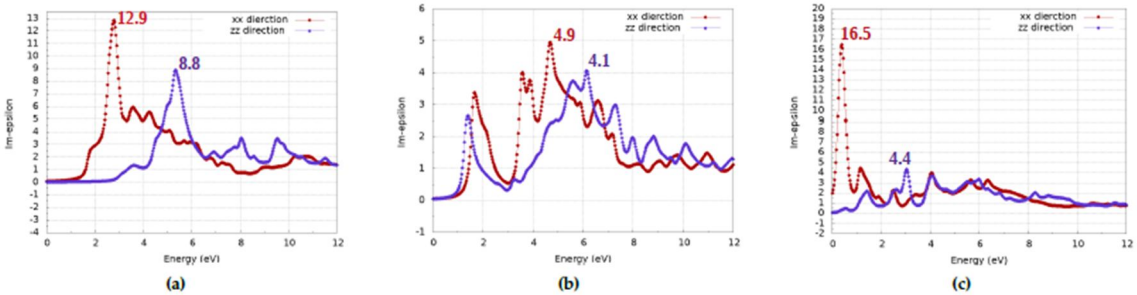

FIG. 5. #2(w) of (a) pristine, (b) Zr-doped, and (c) Zr-N co-doped MoS2 in perpendicular (zz) and parallel (xx) directions.

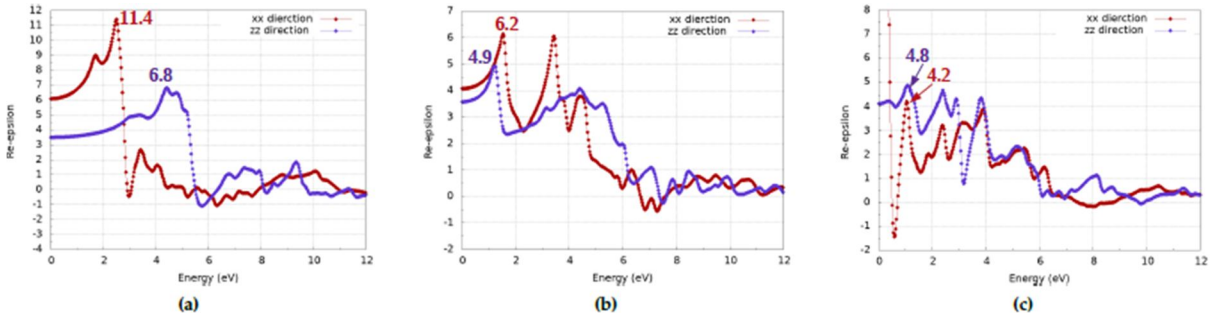

FIG. 6. #1(w) of (a) pristine, (b) Zr-doped, and (c) Zr-N co-doped MoS_2 in perpendicular (zz) and parallel (xx) directions.

TABLE 2. Static refractive index n(0).

Material	$n_{\parallel}(0)$	$n_{\perp}(0)$
MoS_2	2.60	1.85
$Zr\ doped\ MoS_2$	2.30	1.90
$Zr-N\ codoped\ MoS_2$	4.10	2.00

All highest peaks in parallel and perpendicular polarizations are listed in Table 3, corresponding to the pristine, Zr-doped, and Zr-N co-doped MoS_2 monolayer materials. At roughly 6.25 eV, the refractive indices fall below unity in some ranges, which provides the photoluminescence phenomenon, in which the phase velocity of passing light exceeds the speed of light in a vacuum.

4. Conclusion

The structural, electronic, and optical properties of the pristine, Zr-doped, and Zr-N co-doped MoS_2 monolayer were studied by the DFT method with GGA-PBE calculations. The analyses of the formation energy calculations indicate that all doped structures are energetically stable, with the Zr-N co-doped structure being the most stable. More importantly, the band structure results show that the pristine MoS_2 monolayer has a direct band gap of 1.66 eV, which agrees with the experimental results. The band gap decreases after doping with the Zr transition metal and changes its type to an indirect band gap. However, in the case of Zr-N co-doping, the band gap is cancelled, indicating a metallic character for the co-doped structure. The Mo - d, Zr - d, N - p, and S - p orbitals are often responsible for the observed DOS and PDOS profiles. The results also show that the Zr-doping and Zr-N co-doping are practical tools for tuning the pristine MoS_2 monolayer's optical properties. The optical response is completely distinct in the two polarization orientations, suggesting anisotropic optical characteristics, making these materials promising for applications such as linear polarizers. The analyses of the dielectric function show that the $\varepsilon_2(\omega)$ of all studied structures possesses various peaks at different energy regions (IR, VL, and UV regions), indicating the possibility of light absorption in these regions. All investigated structures have refractive indices lower than a unit value in a specified range. The phase velocity of travelling light is greater than the speed of light in a vacuum, resulting in photoluminescence. This study provides valuable insights into the nature of the pristine, Zr-doped, and Zr-N co-doped MoS_2 monolayers and is a powerful tool for experimental research in the future.

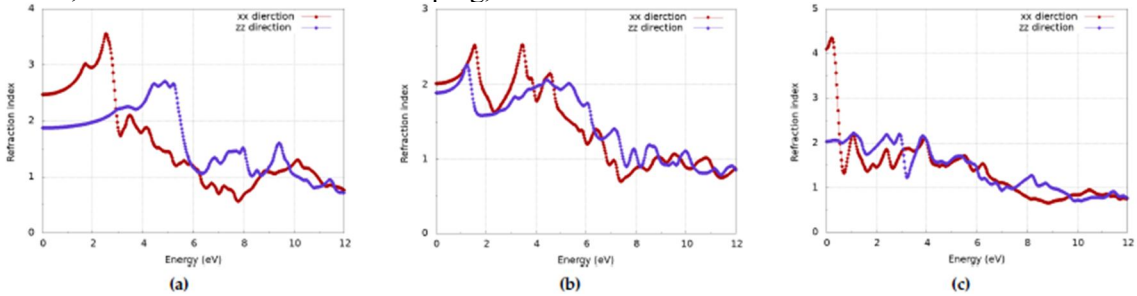

FIG. 7. n(w) of (a) pristine, (b) Zr-doped, and (c) Zr-N co-doped MoS2 in perpendicular (zz) and parallel (xx) directions.

TABLE 3. Energies, polarization states, and spectral region of the refraction index peaks of pristine, Zr-doped, and Zr-N co-doped MoS2 mono-layer materials.

Material	Peaks ∥	Peaks ⊥	Energy [eV]	Spectrum region
MoS_2 monolayer	3.1	-	1.80	VISIBLE
	3.5	-	2.80	VISIBLE
	-	2.60	4.80	UV
	-	2.70	5.00	UV
	-	2.50	5.20	UV
Zr-doped MoS_2	2.60	-	1.50	IR
	2.62	-	3.40	UV
	-	2.22	1.42	IR
	-	2.05	4.25	UV
	-	2.03	5.26	UV
Zr-N codoped MoS_2	4.30	-	0.17	IR
	2.18	-	1.20	IR
	-	2.18	1.20	IR
	-	2.14	2.4	VISIBLE
	-	2.13	2.9	VISIBLE
	-	2.10	3.84	UV

References

[1] Ganta, D., Sinha, S., and Haasch, R.T., Surf. Sci. Spectra, 21 (1) (2014) 19.

[2] Farkad, O., Elfatouaki, F., Takassa, R., Hassine, S., Ijdiyaou, Y., Ibnouelghazi, E., and Abouelaoualim, D., Mater. Today Commun., 33 (2022) 104714.

[3] Farkad, O., Takassa, R., Elfatouaki, F., Hassine, S., Ijdiyaou, Y., Ibnouelghazi, E., and Abouelaoualim, D., Diam. Relat. Mater., 126 (2022) 109082.

[4] Mao, X., Wang, L., Xu, Y., and Li, Y., J. Phys. Chem. C, 124 (19) (2020) 10523.

[5] Ma, H., Shen, Z., and Ben, S., J. Colloid Interface Sci., 517 (2018) 204.

[6] Han, S., Kwon, H., Kim, S.K., Ryu, S., Yun, W.S., Kim, D., Hwang, J., Kang, J.-S., Baik, J., Shin, H., et al., Phys. Rev. B, 84 (4) (2011) 045409.

[7] Wang, A.R., Ruzicka, B.A., Kumar, N., Bellus, M.Z., Chiu, H.-Y., and Zhao, H., Phys. Rev. B, 86 (4) (2012) 045406.

[8] Fang, H., Chuang, S., Chang, T.C., Takei, K., Takahashi, T., and Javey, A., Nano Lett., 12 (7) (2012) 3788.

[9] Yue, Q., Shao, Z., Chang, S., and Li, J., Nanoscale Res. Lett., 8 (1) (2013) 1.

[10] Donarelli, M., Prezioso, S., Perrozzi, F., Bisti, F., Nardone, M., Giancaterini, L., Cantalini, C., and Ottaviano, L., Sens. Actuators B Chem., 207 (2015) 602.

[11] Du, R. and Wu, W., Chem. Phys. Lett., 789 (2022) 139300.

[12] Wu, F., Tian, H., Shen, Y., Hou, Z., Ren, J., Gou, G., Sun, Y., Yang, Y., and Ren, T.-L., Nature, 603 (7900) (2022) 259.

[13] Ullah, M.S., Yousuf, A.H.B., Es-Sakhi, A.D., and Chowdhury, M.H., AIP Conf. Proc., 1957 (2018) 020001.

[14] Omar, O.S., J. Renew. Mater., 10 (7) (2022) 1979.

[15] Kang, M.-A., Kim, S.J., Song, W., Chang, S.-j., Park, C.-Y., Myung, S., Lim, J., Lee, S. S., and An, K.-S., Carbon, 116 (2017) 167.

[16] Qian, G., Peng, Q., Zou, D., Wang, S., Yan, B., and Zhou, Q., Front. Mater., 7 (2020) 22.

[17] Lahourpour, F., Boochani, A., Parhizgar, S., and Elahi, S., J. Theor. Appl. Phys., 13 (3) (2019) 191.

[18] Splendiani, A., Sun, L., Zhang, Y., Li, T., Kim, J., Chim, C.-Y., Galli, G., and Wang, F., Nano Lett. 10 (4) (2010) 1271.

[19] Lebegue, S. and Eriksson, O., Phys. Rev. B, 79 (11) (2009) 115409.

[20] Tenne, R., Angew. Chem. Int. Ed., 42 (42) (2003) 5124.

[21] Hu, A.-M., Wang, L.-l., Xiao, W.-Z., Xiao, G., and Rong, Q.-Y., Comput. Mater. Sci., 107 (2015) 72.

[22] Xu, W.-B., Huang, B.-J., Li, P., Li, F., Zhang, C.-W., and Wang, P.-J., Nanoscale Res. Lett., 9 (1) (2014) 1.

[23] Raza, A., Qumar, U., Haider, A., Naz, S., Haider, J., Ul-Hamid, A., Ikram, M., Ali, S., Goumri-Said, S., and Kanoun, M.B., Dalton Trans., 50 (19) (2021) 6598.

[24] Zhao, X., Xia, C., Wang, T., and Dai, X., J. Alloys Compd., 654 (2016) 574.

[25] Onofrio, N., Guzman, D., and Strachan, A., J. Appl. Phys., 122 (18) (2017) 185102.

[26] Guo, S., Zheng, H., Wang, Y., and Zhang, J., AIP Adv., 9 (7) (2019) 075304.

[27] Takassa, R., Farkad, O., Ibnouelghazi, E., and Abouelaoualim, D., Appl. Surf. Sci., 563 (2021) 150283.

[28] Takassa, R., Farkad, O., Ibnouelghazi, E.A., and Abouelaoualim, D., J. Nano Res., 74 (2022) 1.

[29] Blaha, P., Schwarz, K., Sorantin, P., and Trickey, S.B., Comput. Phys. Commun., 59 (2) (1990) 399.

[30] Blaha, P., Schwarz, K., Madsen, G.K.H., Kvasnicka, D., Luitz, J., Laskowsk, R., Tran, F., Marks, L., and Marks, L., "WIEN2k: An Augmented Plane Wave Plus Local Orbitals Program for Calculating Crystal Properties", (Techn. Universitat, 2019).

[31] Takassa, R., Farkad, O., Ibnouelghazi, E., and Abouelaoualim, D., Diam. Relat. Mater., 123 (2022) 108863.

[32] Elfatouaki, F., Farkad, O., Ibnouelghazi, E., Abouelaoualim, D., and Outzourhit, A., Mater. Sci. Semicond. Process., 143 (2022) 106488.

[33] Hellgren, M. and Baguet, L., Phys. Rev. Res., 3 (2021) 033263.

[34] Blaha, P., Schwarz, K., Tran, F., Laskowski, R., Madsen, G.K.H., and Marks, L.D., J. Chem. Phys., 152 (7) (2020) 074101.

[35] de L. Kronig, R, J. Opt. Soc. Am., 12 (6) (1926) 547.

[36] Kadantsev, E.S. and Hawrylak, P., Solid State Commun., 152 (10) (2012) 909.

[37] Obodo, K.O., Ouma, C.N.M., Obodo, J.T., Braun, M., and Bessarabov, D., Comput. Condens. Matter, 21 (2019) e00419.

[38] Mak, K.F., Lee, C., Hone, J., Shan, J., and Heinz, T.F., Phys. Rev. Lett., 105 (2010) 136805.

[39] Murnaghan, F.D., Proc. Natl. Acad. Sci., 30 (9) (1944) 244.

[40] Ivanovskaya, V.V., Zobelli, A., Gloter, A., Brun, N., Serin, V., and Colliex, C., Phys. Rev. B, 78 (13) (2008) 134104.

[41] Wooten, F., Am. J. Phys., 41 (7) (1973) 939.

[42] Gajdoš, M., Hummer, K., Kresse, G., Furthmüller, J., and Bechstedt, F., Phys. Rev. B, 73 (4) (2006) 045112.

[43] Adler, S.L., Phys. Rev., 126 (2) (1962) 413.

[44] Wiser, N., Phys. Rev., 129 (1) (1963) 62.

[45] Alrashdi, O., Asif, A., Fadhali, M.M., Bakar, A., Afaq, A., and Alqahtani, J., J. Mater. Res. Technol., 20 (2022) 4220.

[46] Takassa, R., Elfatouaki, F., Farkad, O., Hassine, S., Choukri, O., Mouncharih, A., Ijdiyaou, Y., Ibnouelghazi, E., and Abouelaoualim, D., Phys. E Low-Dimens. Syst. Nanostruct., 148 (2023) 115627.